First measurement of proton's charge form-factor at very low Q^2 with initial state radiation

M. Mihovilovič,[1,2] A. B. Weber,[1] P. Achenbach,[1] T. Beranek,[1] J. Beričič,[2] J. C. Bernauer,[3] D. Bosnar,[4] R. Böhm,[1] M. Cardinali,[1] L. Correa,[1] A. Denig,[1] M. O. Distler,[1] A. Esser,[1] M. I. Feretti Bondy,[1] H. Fonvieille,[5] J. Friedrich,[1] I. Friščić,[4] K. Griffioen,[6] M. Hoek,[1] S. Kegel,[1] Y. Kohl,[1] D. G. Middleton,[1] H. Merkel,[1,*] U. Müller,[1] J. Pochodzalla,[1] B. S. Schlimme,[1] M. Schoth,[1] F. Schulz,[1] C. Sfienti,[1] S. Širca,[7,2] S. Štajner,[2] M. Thiel,[1] A. Tyukin,[1] and M. Vanderhaeghen[1]

(A1 Collaboration)

[1] *Institut für Kernphysik, Johannes Gutenberg-Universität Mainz, DE-55128 Mainz, Germany*
[2] *Jožef Stefan Institute, SI-1000 Ljubljana, Slovenia*
[3] *Massachusetts Institute of Technology, Cambridge, MA 02139, USA*
[4] *Department of Physics, University of Zagreb, HR-10002 Zagreb, Croatia*
[5] *Clermont Université, Université Blaise Pascal, F-63000 Clermont-Ferrand, France*
[6] *College of William and Mary, Williamsburg, VA 23187, USA*
[7] *Department of Physics, University of Ljubljana, SI-1000 Ljubljana, Slovenia*

(Dated: March 2, 2016)

This paper reports on a new experimental method based on initial state radiation (ISR), which, exploiting the information inside the radiative tail of the elastic *e*-*p* peak, offers the possibility for precise measurement of the proton charge form factor (G_E^p) at extremely small Q^2. The ISR technique was validated in a dedicated experiment with the spectrometers of the A1-Collaboration at the Mainz Microtron (MAMI) and provided first measurements of the G_E^p at $0.001\,(\mathrm{GeV}/c)^2 \leq Q^2 \leq 0.004\,(\mathrm{GeV}/c)^2$.

PACS numbers: 12.20.-m, 25.30.Bf, 41.60.-m

INTRODUCTION

The proton's radius has been determined by various electron scattering experiments [1–3] and atomic Lamb shift measurements [4–8]. Both approaches gave consistent results. Their average [9], however, does not agree with the findings of very precise Lamb shift measurements in muonic hydrogen [10, 11], which is $7.9\,\sigma$ away from the previously accepted value. This discrepancy cannot be explained within the existing physics theories, nor could it be interpreted as an experimental error. To provide further insight into the matter several new spectroscopic and scattering experiments are underway, which aim to investigate different aspects of the problem [12, 13].

In a scattering experiment the charge radius of the proton is typically determined indirectly by measuring the cross-section for elastic scattering of electrons off hydrogen, which depends on G_E^p and carries information about the charge distribution in the proton. The proton charge radius is defined as:

$$r_e^2 \equiv -\frac{\hbar^2}{6}\frac{dG_E^p}{dQ^2}\bigg|_{Q^2=0}\,, \tag{1}$$

where Q^2 represents the square of the four-momentum transferred to the proton. Due to limited reach of available data sets ($Q^2 > 0.004\,\mathrm{GeV}^2/c^2$) the radius cannot be calculated directly, but needs to be extracted from the initial slope of a model fitted to the measurements. Although the existing data have enough resolving power to precisely determine the slope of the form-factor, past experiments were all missing precise enough information on the absolute scale of the data, needed to constrain the model at $Q^2 = 0$. In their analyses the global normalization factor was treated as a free parameter and was determined by extrapolating the measurements to $Q^2 \to 0$ and matching the theoretical limit $G_E^p(Q^2 = 0) = 1$. Consequently, their results on the proton charge radius depend strongly on the employed model and details of the extrapolation. To abolish such ambiguities, measurements of G_E^p need to be extended to $Q^2 \lesssim 10^{-3}\,(\mathrm{GeV}/c)^2$, where the form-factor is practically one, thus can be exploited as an effective normalization point.

Unfortunately efforts to do such measurement with the standard approaches are limited by the minimal Q^2 accessible by the utilized experimental apparatus, which is bound by the minimal possible energy of the electron beam and the smallest possible scattering angle. Here we present a new experimental approach, that avoids these kinematic limitations, extends the currently accessible Q^2 range and allows for cross-section measurement below $0.004\,(\mathrm{GeV}/c)^2$ with a sub-percent precision. The technique, called initial state radiation technique (ISR) exploits information stored inside the radiative tail of the elastic peak and was inspired by a similar concept used in the particle physics to measure e^+e^- cross sections into hadrons over a wide range of center-of-mass energies in a single experiment [14, 15].

INITIAL STATE RADIATION TECHNIQUE

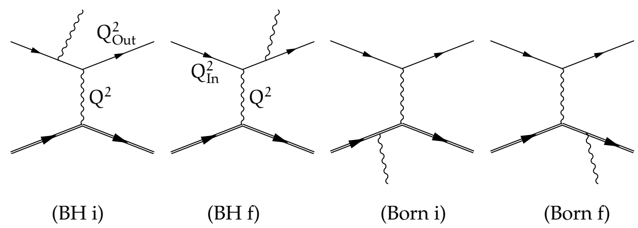

FIG. 1. Feynman diagrams for inelastic scattering of electron off a proton, where the electron and proton emit real photons before or after the interaction. Diagrams where electrons emit a photon are known as Bethe-Heitler (BH) diagrams, while those where protons emit real photons are called Born diagrams. The Q^2 represents the square of the four-momentum transferred to the hadron. The $Q^2_{\rm In}$ is the momentum fixed by the beam energy and the scattering angle, while the $Q^2_{\rm Out} \leq Q^2_{\rm In}$ corresponds to value measured with the detector. For the (BH-i) $Q^2 = Q^2_{\rm Out}$, and for the (BH-f) $Q^2 = Q^2_{\rm In}$.

The radiative tail of an elastic peak is dominated by contributions of two Bethe-Heitler diagrams [16] shown in Figure 1: the initial state radiation (BH i) where the incident electron emits a real photon before interacting with the proton, and the final state radiation (BH f), where the real photon is emitted only after the interaction with the nucleon. For these processes two characteristic squares of four-momenta can be defined:

$$Q^2_{\rm In} = \frac{4E_0^2 \sin^2\frac{\theta_{e'}}{2}}{1+\frac{E_0}{2M}\sin^2\frac{\theta_{e'}}{2}}\,, \qquad Q^2_{\rm Out} = \frac{4E'^2 \sin^2\frac{\theta_{e'}}{2}}{1-\frac{E'}{2M}\sin^2\frac{\theta_{e'}}{2}}\,.$$

$Q^2_{\rm In}$ represent the value set by the chosen kinematics for elastic scattering (E_0, θ_e'), while $Q^2_{\rm Out}$ corresponds to the value measured by the detectors. E_0 and E' are the energies of the incoming and scattered electron, M is the mass of the proton, and $\theta_{e'}$ is the scattering angle of the detected electron. While in the limit of elastic $\mathrm{H(e,e')p}$ scattering $Q^2_{\rm In} = Q^2_{\rm Out}$ and correspond to the momentum Q^2 transfered to the proton, in $\mathrm{H(e,e')}\gamma\mathrm{p}$ reactions they no longer agree. In the initial state radiation diagram the emitted photon carries away part of the incident electron's four-momentum and opens the possibility to probe the proton's electromagnetic structure at $Q^2 = Q^2_{\rm Out}$ that is smaller than the $Q^2_{\rm In}$. On the other hand, in the final state radiation diagram momentum transfer at the vertex remains fixed ($Q^2 = Q^2_{\rm In}$), and only the detected $Q^2_{\rm Out} \leq Q^2$ changes.

In an inclusive experiment only $Q^2_{\rm Out}$ can be measured, which means that looking only at data, initial state radiation processes cannot be distinguished from the final state radiation. Hence, the measured radiative tail represents approximately a 40/60 mixture of terms with form-factors at $Q^2 = Q^2_{\rm In}$ known by elastic measurements and unknown form-factors at $Q^2 = Q^2_{\rm Out}$. There are also Born terms (Born-i and Born-f), where the initial and final proton emit real photons, and higher order vertex and radiative corrections that also contribute to the radiative tail. The basic concept of the ISR approach is to isolate the interesting (BH-i) process from other contributions to the radiative tail and by this way reach information on form-factors at yet unmeasured Q^2. To accomplish this the measurements need to be studied in conjunction with a Monte-Carlo simulation that encompasses a comprehensive description of all Feynman diagrams relevant to the radiative tail.

DESCRIPTION OF RADIATIVE TAIL

To realistically mimic the radiative tail the peaking approximation models devised from the corrections to the elastic cross-section [16] are insufficient. For an adequate description far away from the elastic line ($Q^2_{\rm Out} \ll Q^2_{\rm In}$), it is crucial to consider diagrams to the α^4-order. To achieve this goal, a Monte-Carlo simulation is used, which employs a sophisticated event generator, that exactly calculates amplitudes [16] for the leading, α^3-order diagrams (Figure 1) and includes G_E^p as a free, tunable parameter. The next order vacuum polarization diagrams (with electrons inside the lepton loop) are exactly calculable and can be added as an multiplicative factor to the cross-section. The virtual corrections to the Bethe-Heitler diagrams (self energy corrections and various vertex corrections) require integration of the loop diagrams and are computationally too intensive to be added directly to the simulation. Instead they are considered as effective corrections to the cross-section using prescription of [16], together with the real second-order correction (emission of two real photons) which is approximated with the corrections to the elastic cross-section [16, 17]. The corrections on the hadronic side are also considered in the elastic limit by using the calculations of [17] and contribute only up to 0.5 % to the cross-section at the lowest energy settings. In the simulation, the proton is always on-shell. The effects related to the internal structure of the proton, described with the general polarisabilities [18] and known from the VCS experiments [19], were at given Q^2 determined to be tiny and could be neglected. Beside the internal corrections, the simulation includes also external radiative corrections [20], considers collisional losses of particles on their way from the vertex point to the detectors, and implements the precise acceptances of the spectrometers.

To determine the form-factor that reproduces the measured radiative tail, the simulation needs to be performed for different values of G_E^p to find such that fits simulation best to the data. The contribution of G_M^p to the cross-section is at $Q^2 \leq 10^{-2}\,\mathrm{GeV^2/c^2}$ smaller than 0.5 % and can therefore be approximated with the standard dipole approximation and considered only as a correction to the cross-section.

EXPERIMENT

To validate the feasibility of the ISR approach, a detailed measurement of the radiative tail has been performed at Mainz Microtron (MAMI) in 2013 using the spectrometer setup of the A1-Collaboration [21]. In the experiment a rastered electron beam with energies of 195 MeV, 330 MeV and 495 MeV was used in combination with a hydrogen target, which consisted of a thin 5 cm long cigar shaped Havar cell filled with liquid hydrogen (LH_2), inserted into the evacuated scattering chamber. For cross-section measurements a single dipole magnetic spectrometer B with the energy acceptance of $\pm 7.5\,\%$ was employed. It was positioned at a fixed angle of 15.21°, while its energy settings were being adjusted to scan the complete radiative tail for each energy setting. The central energy of each setting was measured with the NMR probe with a relative accuracy of 8×10^{-5}. For detection of particles spectrometer utilized a detector package consisting of two layers of vertical-drift-chambers for tracking, two layers of scintillation detectors for triggering and a threshold Cerenkov detector for particle-identification. Kinematic settings of the experiment were chosen such that the radiative tails of all three settings overlap. In total, 42 different setups were devised, resulting in three weeks of data taking.

The beam current between 10 nA and 1 μA was limited by the maximum rate allowed in the VDCs ($\approx$ 1 kHz/wire), resulting in raw rates up to 20 kHz. The current was determined by non-invasive fuxgate-magnetometer and from the collected charge of the stopped beam. Unfortunately at low beam currents and low beam energies the accuracy of both approaches is $\geq 2\,\%$, which is insufficient for a precision cross-section measurement. Hence spectrometer A positioned at a fixed setting was employed for precise monitoring of the beam luminosity.

In spite of the good vacuum conditions inside the scattering chamber (10^{-6} mbar), the experiment was sensitive to traces of cryogenic depositions on the target walls, consisting mostly of residual nitrogen and oxygen present in the scattering chamber [22]. Since the deposed layer affected the measured spectra, the kinematic settings for spectrometer A were chosen such, that the nitrogen/oxygen elastic lines were always visible next to the hydrogen spectrum, and served as a precise monitor of the thickness of the cryogenic depositions.

The data were collected with 800 Hz and with a livetime of $\approx 50\,\%$. Each collected data sample contains $\approx$ 2 M evens and consists of measurements of the radiative tail for a chosen E' range collected with spectrometer B and a corresponding reference (luminosity) spectrum from spectrometer A.

DATA ANALYSIS

The measurements at highest two beam energy settings enclose data at Q^2, where G_E^p is known from previous experiments and were used for validation of ISR technique. The measurements with beam energy of 195 MeV were made to investigate G_E^p at yet unmeasured Q^2.

Before comparing the data to the simulation, the measured spectra had to be corrected for the inefficiencies of the detection system. The efficiencies of the Scintillation detector and Cherenkov detector were determined to be $99.8 \pm 0.2\,\%$ and $99.74 \pm 0.02\,\%$, respectively, and were considered as multiplicative correction factors to the measured distributions. The quality of the agreement between the data and simulation depends also on the momentum and spatial resolutions of the spectrometer. They were determined from dedicated calibrations data-sets. The obtained relative momentum, angular and vertex resolutions (FWHM) were 1.7×10^{-4}, 3 msr and 1.6 mm, respectively.

A series of cuts was applied to the data in order to minimize the background. First, a cut on the Cherenkov signal was applied to identify electrons, followed by a cut on the nominal momentum acceptance of the spectrometer. To minimize the contributions of events coming from the target walls and cryogenic depositions, a strict, ± 10 mm cut on the vertex position was applied. Due to the finite vertex resolution some of the background events remain in the cut sample. Their contributions to the spectra was estimated by using a dedicated simulation, normalized to the size of the nitrogen/oxygen elastic line, and corrected for the changes in the thickness of the depositions using data of Spectrometer A.

The most challenging background were events coming from the frame of the entrance window of spectrometer B. When measuring far away from the elastic peak, the elastically scattered electrons, which a priori cannot enter the acceptance, undergo secondary processes in the metal parts of the entrance flunge and re-scatter back into the acceptance of the spectrometer. At high E' these contributions are negligible, but at low E', where the cross section for the Bethe-Heitler processes becomes comparable to the probability for double scattering processes, these secondary reactions begin to contribute substantially to the detected number of events. At high beam-energy settings, the background can be successfully removed via strict vertex cuts. However, at the lowest energy settings, a substantial part remained inside the data and limited our efforts in measuring the proton charge form-factor. Since this background could not be adequately subtracted or simulated, the data below $E' < 128$ MeV were omitted from the present analysis, thus limited the reach of the experiment to $Q^2 \geq 1.3 \cdot 10^{-3}\,\mathrm{GeV}^2/\mathrm{c}^2$.

The cleaned samples of events for individual kinematic setting were corrected for the dead-time and prescale factors, weighted with the relative luminosity determined with spectrometer A and then merged together to form a single spectrum , that could be compared to the simulation (see Fig. 2) ran with the spline parameterization [1] of the G_E^p form-factor (currently best). For each beam-energy settings a golden datum was selected which served as a reference for the relative normalization of luminosity for other data sets. Hence, for each beam-energy one free parameter (absolute normalization) remained unknown, which was then determined by normalizing the ratio between the data and simulation to one.

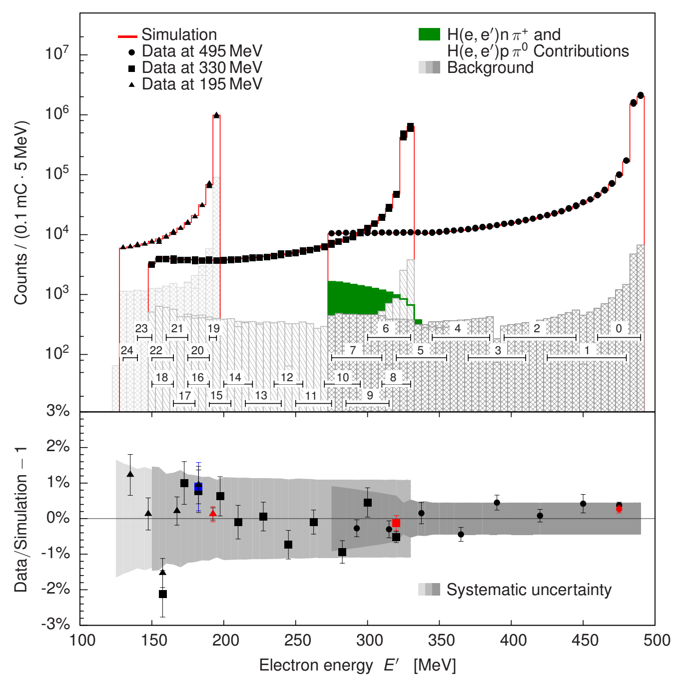

FIG. 2. Comparison of the data to the simulation. (top) Circles (squares, triangles) show the measured distributions for the 495 MeV (330 MeV, 195 MeV) setting, normalized to 0.1 mC. The elastic peak is followed by a long radiative tail. The simulation performed with form-factor parameterization of [1] is shown with a blue line. The measurements at 495 MeV, 330 MeV, 195 MeV were divided into eight $(0-7)$, eleven $(8-18)$ and six $(19-24)$ energy ranges, respectively, such that two neighboring settings overlap for 1/2 of the energy acceptance. The residual contributions of target walls and cryogenic depositions are shown with dashed fields. The full fields represent the effects of the pion production processes. (bottom) Relative difference between the data and simulation. The points show the mean values for each kinematic point, while the error bars on the points denote the statistical uncertainty of the mean value. Gray bands demonstrate the systematical uncertainties. (Colors on-line)

In the bins far away from the elastic peak, one also needs to consider $\mathrm{H(e,e')n\pi^+}$ and $\mathrm{H(e,e')p\pi^0}$ reactions, which contribute up to 10 % of all events. These processes were considered in terms of the MAID model [23] and were added to the full simulation before comparing it to the data. The final level of agreement between the data and simulation is shown on the Fig. 2 (bottom).

SYSTEMATIC UNCERTAINTIES

An advantage of the ISR technique is an extremely good control over the systematic uncertainties. With the fixed angular settings and overlapping momentum ranges all ambiguities related to the acceptances disappear. Furthermore, with spectrometer A one directly measures the luminosity, thus avoiding potential problems with fluctuations in beam current and target density, leading to a relative luminosity determination with an accuracy better than 0.17 %. Other sources of systematic uncertainty are: the ambiguity in the determination of detector efficiencies of 0.2 %; the inconclusiveness of the background simulation at lowest momenta, which is smaller than 0.24 %; the contribution of the higher order corrections to the simulation, which are not included in the simulation, is 0.36 %. The bins including pion production events are subjected to another 0.5 %, due to uncertainties of the MAID model near the threshold. This contribution, which appears to be the leading source of the systematic uncertainty, is significant only for the 495 MeV setting. For the measurements at 195 MeV and 330 MeV is the contribution of pion production processes $\leq 2\,\%$ and the corresponding systematic uncertainty $\leq 0.1\,\%$.

RESULTS AND OUTLOOK

For the two highest energy settings Fig. 2 exhibits a better than a percent agreement between the data and simulation in the region, that extends more than 200 MeV from the elastic line. Assuming correct description of the form-factors this demonstrates for the first time that electro-magnetic processes which give rise to the radiative tail are understood to a few per-mil level. This is crucial for the interpretation of experiments which results strongly depend on the quality of radiative corrections [27]. Substituting the existing parameterization of G_E^p with an open parameter model, independent values for the proton-charge form-factor in the region of $0.001\,(\mathrm{GeV}/c)^2 \leq Q^2 \leq 0.017\,(\mathrm{GeV}/c)^2$ could be determined. The new values shown in Fig. 3 are in good agreement with results of previous measurements [1, 24–26]. This proves the principle of initial state radiation as a viable method for precise investigation of the electromagnetic structure of the nucleon at extremely small Q^2 and motivates further experiments of this kind. Finally, the extracted values for G_E^p were fitted with two parameter dipole function $G(Q^2) = n/(1+Q^2/a)^2$, resulting in $a = (0.657 \pm 0.033)\,\mathrm{GeV}^2/\mathrm{c}^2$ and $n = 1.002 \pm 0.001$. Using this result in Eq. 1, a proton charge radius of

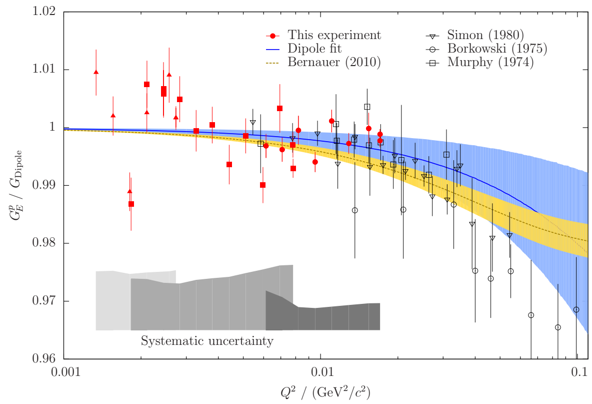

FIG. 3. The G_E^p normalized to the standard dipole $G_D = (1 + \frac{Q^2}{0.71\,\mathrm{GeV}^2/c^2})^{-2}$ as a function of Q^2. Empty black points show values of previous experiments [24–26]. Dashed line with corresponding error-band represents current best form-factor parameterization by [1]. Results of this experiment are shown with full circles and the full line represents the dipole fit to these data. Band around the line demonstrates the uncertainty of the fit. Gray structures at the bottom demonstrate the size of the systematic uncertainties for the three energy settings. (Colors on-line)

$r_e = (0.843 \pm 0.021_{\mathrm{stat.}} \pm 0.004_{\mathrm{sys.}})\,\mathrm{fm}$ was calculated. Due to the sheared E' reach of the experiment is the obtained value is inferior to best radius measurement [3], but supports the hypothesis of a smaller radius.

The authors would like to thank the MAMI accelerator group for the excellent beam quality which made this experiment possible. This work is supported by the Federal State of Rhineland-Palatinate and by the Deutsche Forschungsgemeinschaft with the Collaborative Research Center 1044.

* merkel@kph.uni-mainz.de

[1] J. C. Bernauer *et al.*, Phys. Rev. Lett. **105**, 242001 (2010).
[2] X. Zhan *et al.*, Physics Letters B **705**, 59 (2011).
[3] J. C. Bernauer *et al.*, Phys. Rev. C **90**, 015206 (2014).
[4] S. R. Lundeen and F. M. Pipkin, Phys. Rev. Lett. **46**, 232 (1981).
[5] E. W. Hagley and F. M. Pipkin, Phys. Rev. Lett. **72**, 1172 (1994).
[6] U. Jentschura and K. Pachucki, Phys. Rev. A **54**, 1853 (1996).
[7] M. Weitz, A. Huber, F. Schmidt-Kaler, D. Leibfried, and T. W. Hänsch, Phys. Rev. Lett. **72**, 328 (1994).
[8] T. Udem, A. Huber, B. Gross, J. Reichert, M. Prevedelli, M. Weitz, and T. W. Hänsch, Phys. Rev. Lett. **79**, 2646 (1997).
[9] P. J. Mohr, B. N. Taylor, and D. B. Newell, Journal of Physical and Chemical Reference Data **41**, 043109 (2012).
[10] R. Pohl *et al.*, Nature **466**, 213 (2010).
[11] A. Antognini *et al.*, Science **339**, 417 (2013).
[12] R. Pohl, R. Gilman, G. A. Miller, and K. Pachucki, Ann. Rev. Nucl. Part. Sci. **63**, 175 (2013), arXiv:1301.0905 [physics.atom-ph].
[13] C. E. Carlson, Progress in Particle and Nuclear Physics **82**, 59 (2015).
[14] A. B. Arbuzov, E. A. Kuraev, N. P. Merenkov, and L. Trentadue, Journal of High Energy Physics **1998**, 009 (1998).
[15] B. Aubert *et al.* (BABAR Collaboration), Phys. Rev. D **69**, 011103 (2004).
[16] M. Vanderhaeghen, J. M. Friedrich, D. Lhuillier, D. Marchand, L. Van Hoorebeke, and J. Van de Wiele, Phys. Rev. C **62**, 025501 (2000).
[17] L. C. Maximon and J. A. Tjon, Phys. Rev. C **62**, 054320 (2000).
[18] H. Arenhövel and D. Drechsel, Nucl. Phys. A **233**, 153 (1974).
[19] J. Roche *et al.*, Phys. Rev. Lett. **85**, 708 (2000).
[20] L. W. Mo and Y. S. Tsai, Rev. Mod. Phys. **41**, 205 (1969).
[21] K. Blomqvist *et al.*, Nucl. Instr. and Meth. A **403**, 263 (1998).
[22] M. Mihovilovic *et al.*, EPJ Web Conf. **72**, 00017 (2014).
[23] D. Drechsel, S. Kamalov, and L. Tiator, The European Physical Journal A **34**, 69 (2007).
[24] G. Simon, C. Schmitt, F. Borkowski, and V. Walther, Nuclear Physics A **333**, 381 (1980).
[25] J. J. Murphy, Y. M. Shin, and D. M. Skopik, Phys. Rev. C **9**, 2125 (1974).
[26] F. Borkowski, P. Peuser, G. Simon, V. Walther, and R. Wendling, Nuclear Physics A **222**, 269 (1974).
[27] P. Janssens *et al.*, The European Physical Journal A **37**, 1 (2008).